JOURNAL OF THEORETICAL
AND APPLIED MECHANICS
61, 3, pp. 427-439, Warsaw 2023
https://doi.org/10.15632/jtam-pl/165949

STUDY ON THE ISOLATION EFFECT OF A COMPOSITE MULTILAYER WAVE IMPEDING BLOCK ON THE *S*-WAVE IN AN UNSATURATED FOUNDATION

Ye Jiang
School of Civil Engineering, Qinghai University, Xining, China
Qiang Ma, Yan-Hong Bao
School of Civil Engineering, Qinghai University, Xining, China, and
Qinghai Provincial Key Laboratory of Energy-Saving Building Materials and Engineering Safety, Xining, China
corresponding author Qiang Ma, e-mail: maqiang0104@163.com

The traditional wave impeding block (WIB) is improved to a composite multilayer WIB with the same thickness (tri-layer as an example). Firstly, a physical model of the composite multilayer WIB installed in an unsaturated foundation is established, and the isolation effect on the S-wave is studied based on the wave theory in unsaturated porous and elastic media. The purpose of this study is to enhance the isolation frequency of WIB and to show the best isolation effect achieved by selecting the appropriate wave impedance ratio. The influence of saturation on its vibration isolation effect is also analyzed.

Keywords: unsaturated foundation, composite multilayer WIB, environmental vibration isolation

1. Introduction

With the rapidly developing industry and transportation, while improving people's living quality, artificial vibration problems caused by various industrial activities and traffic operations seriously impact structures, precision instruments, and people's normal lives. Therefore, it is of great practical significance to study vibration damping and isolation measures for unsaturated foundations under environmental vibration.

There is no wave propagation in soil when the excitation frequency is lower than the cut-off frequency. In this principle, Chouw *et al.* (1991a,b) was first to propose that a hard interlayer installed in the foundation forms a finite size artificial bedrock for vibration isolation, which is named the wave impeding block (WIB). Yang and Hung (1997) compared the vibration isolation effect of an open trench and WIB under a moving load in an elastic foundation. The results showed that WIB has a better vibration isolation effect. Takemiya and Jiang (1993) established a numerical model of WIB vibration isolation and found that WIB had a better vibration isolation effect at a low frequency below 15.3 Hz. Li *et al.* (2011) compared the vibration isolation effect of the entity wave impeding block (EWIB) and the honeycomb wave impeding block (HWIB) in the elastic foundation and concluded that HWIB had a better vibration isolation effect. But EWIB was more effective for low-frequency vibration at 0-10 Hz. Zhou *et al.* (2016) and Ma *et al.* (2019) investigated the ground vibration control with a fluid-saturated porous WIB and graded WIB, and the results showed that the two types of WIB were superior than a single-phase traditional WIB. Tian *et al.* (2019) and Gao *et al.* (2021) investigated the vibration isolation effect of Duxseal materials in 2D homogeneous elastic foundations and proposed the method of combined vibration isolation by filling Duxseal in the WIB. The results showed that DXWIB could improve the frequency bandwidth of vibration damping, and the vibration isolation effect was better in the range of 5-70 Hz. However, although the above-mentioned studies show that a non-homogeneous WIB can improve the vibration isolation efficiency and performance compared with the conventional WIB, these studies treat the foundation as an elastic or saturated two--phase medium to simplify the complex dynamic problem, which is far from actual engineering.

In the actual engineering, most of foundations are unsaturated soils, and the variation of saturation has a significant influence on vibration wave propagation characteristics. Vibration control measures for unsaturated foundations need to be further studied. Therefore, Shu and Ma (2022) and Shu *et al.* (2022) investigated propagation characteristics of the P_1-wave passing through a single-layer and multilayer WIB in unsaturated foundations, respectively, and the results showed that the wave impedance ratio, shear modulus and density of the WIB material had a significant influence on the transmission and reflection amplitude ratio. Jiang and Ma (2022) investigated the vibration isolation performance of a single-layer WIB in an unsaturated foundation under S-wave incidence. The findings showed that the vibration isolation effect of WIB increased with an increase in saturation, and the single-layer WIB failed to isolate the middle and high frequencies. To enhance the frequency range for vibration isolation of WIB in the unsaturated foundation, according to the literature (Sun and Li, 2011), it is known that the more significant the difference between the interfaces of multilayer and thin-layer, the more significant the vibration wave transmission and reflection effect. Hence, this paper proposes an innovative vibration isolation system with a composite multilayer WIB as a barrier. Based on the wave propagation theory in an unsaturated porous medium and a single-phase elastic medium, and Snell's theorem, the vibration isolation performance of the composite multilayer WIB in the unsaturated foundation under the S-wave incidence is investigated. The analytical solution of the surface vertical displacement after the S-wave incident from the bedrock to the unsaturated soil through the composite multilayer WIB is derived. According to numerical calculations, the influence of the wave impedance ratio at the interface between the unsaturated soil and WIB and that between the layers of composite multilayer WIB on its vibration isolation effect were analyzed, and the isolation effect of single-layer and composite multilayer WIB installed in the unsaturated foundation were compared. The influence laws of various parameters such as the incidence angle, incidence frequency and saturation on the vibration isolation effect of the composite multilayer WIB in the unsaturated foundation were analyzed, thereby providing a guideline for the application of the composite multilayer WIB vibration isolation in unsaturated foundations.

2. Wave equation in unsaturated porous media

This paper is based on the mixture theory of unsaturated porous media (Borja, 2006; Chen *et al.*, 2011). The wave equation of a triphase solid-liquid-gas is expressed as follows. The solid, liquid and gas phases in unsaturated soil layers are indicated by subscripts: S, L and G, respectively

$$
\begin{aligned}
&n^S\rho^S\ddot{\varphi}^S = (\gamma_{SS} + n^S\lambda_S + 2n^S\mu_S)\nabla^2\varphi_S + \gamma_{SL}\nabla^2\varphi_L + \gamma_{SG}\nabla^2\varphi_G \\
&\qquad + \xi_L(\dot{\varphi}_L - \dot{\varphi}_S) + \xi_G(\dot{\varphi}_G - \dot{\varphi}_S) \\
&n^L\rho^L\ddot{\varphi}^L = \gamma_{SL}\nabla^2\varphi_S + \gamma_{LL}\nabla^2\varphi_L + \gamma_{LG}\nabla^2\varphi_G - \xi_L(\dot{\varphi}_L - \dot{\varphi}_S) \\
&n^G\rho^G\ddot{\varphi}^G = \gamma_{SG}\nabla^2\varphi_S + \gamma_{LG}\nabla^2\varphi_L + \gamma_{GG}\nabla^2\varphi_G - \xi_G(\dot{\varphi}_G - \dot{\varphi}_S) \\
&n^S\rho^S\ddot{\psi}_S = n^S\mu_S\nabla^2\psi_S + \xi_L(\dot{\psi}_L - \dot{\psi}_S) + \xi_G(\dot{\psi}_G - \dot{\psi}_S) \\
&n^L\rho^L\ddot{\psi}_L = -\xi_L(\dot{\psi}_L - \dot{\psi}_S) + \xi_G(\dot{\psi}_G - \dot{\psi}_S) \\
&n^G\rho^G\ddot{\psi}_G = -\xi_G(\dot{\psi}_G - \dot{\psi}_S)
\end{aligned}
\tag{2.1}
$$

where n^α (throughout this paper, the character $\alpha = S, L, G$) indicates the initial volume occupied by the α phase. ρ^α denotes the actual mass density of the α phase. ∇^2 represents the Laplace operator in the Cartesian coordinate. The expressions of γ_{SS}, γ_{LL}, γ_{GG}, γ_{SL}, γ_{SG} and γ_{LG} are given in the literature (Chen *et al.*, 2011). ξ_L and ξ_G are the drag force parameters representing the viscous dissipation between the fluids (liquid and gas) and the solid skeleton, respectively.

The general solutions to Eqs. (2.1) are assumed to be

$$\varphi_\alpha = A_\alpha \exp[\mathrm{i}k_p(lx + nz - c_p t)] \qquad \psi_\alpha = B_\alpha \exp[\mathrm{i}k_s(lx + nz - c_s t)] \tag{2.2}$$

where $\mathrm{i} = \sqrt{-1}$. l and n denote the direction vectors of the respective waves. k_p and k_s are the wave numbers of the P-waves and the SV-wave. c_p and c_s are the phase velocities of the P-waves and the SV-wave, respectively.

Substituting Eqs. (2.2) into Eqs. (2.1), the P_1-, P_2-, P_3- and SV-wave velocities in an unsaturated foundation can be obtained.

3. Physical model

The horizontal semi-infinite bedrock is covered by an unsaturated soil layer whose thickness is H. A composite multilayer WIB whose thickness is $H_{w1} + H_{w2} + H_{w3}$ and burial depth H_2 is embedded in the unsaturated foundation. Assuming that the S-wave with frequency ω is incident at any angle φ to the WIB in the unsaturated foundation, the transmission and reflection are shown in Fig. 1.

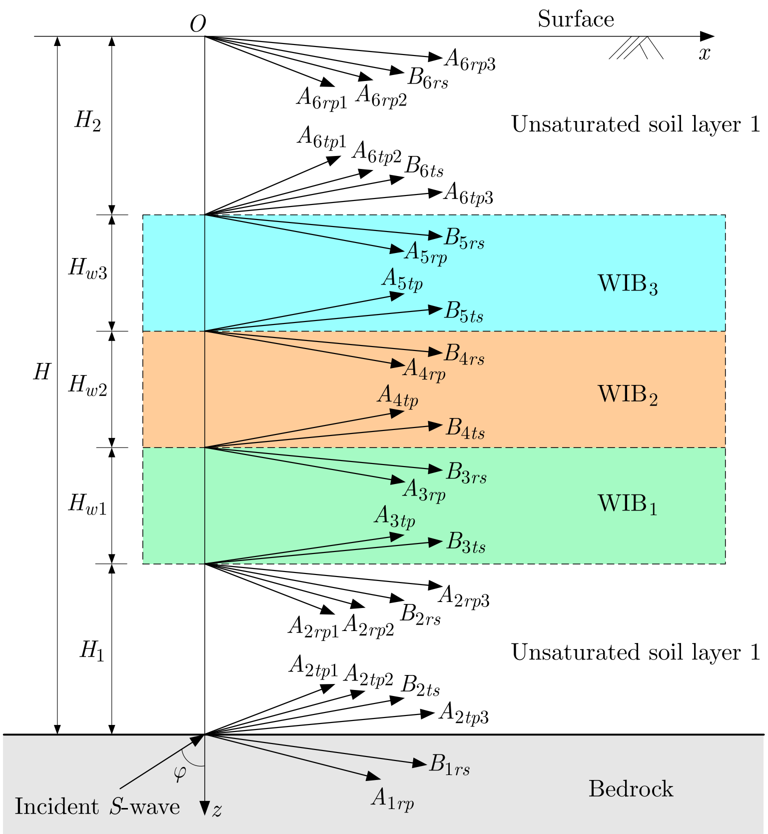

Fig. 1. Propagation of the S-wave when setting the composite multilayer WIB in an unsaturated foundation

4. Analysis of the total wavefield

The bedrock and composite multilayer WIB are simulated with a single-phase elastic medium, and the unsaturated foundation is simulated with an unsaturated porous medium. The wave field in the two-dimensional xz-plane is obtained as we can obtain one compressional wave: P-wave and one shear wave: SV-wave in the single-phase medium, and three compressional: P_1-, P_2- and P_3-waves as well as one shear: SV-wave in the unsaturated porous medium.

4.1. Wave potential functions

The displacement potential functions of the up-going and down-going waves can be indicated as below.

(1) In the bedrock

$$\begin{aligned}
\varphi_1^e &= A_{1rp}\exp[\mathrm{i}(\omega t - k_{1rpx}x - k_{1rpz}z)]\\
\psi_1^e &= B_{1is}\exp[\mathrm{i}(\omega t - k_{1isx}x + k_{1isz}z)] + B_{1rs}\exp[\mathrm{i}(\omega t - k_{1rsx}x - k_{1rsz}z)]
\end{aligned} \tag{4.1}$$

(2) In unsaturated soil layers I and II

The solid phase can be indicated as

$$\begin{aligned}
&\mathrm{I}:\begin{cases}
\varphi_2^S = \sum\limits_{i=1}^{3}\Big\{A_{2tpi}\exp[\mathrm{i}(\omega t - k_{2tpix}x + k_{2tpiz}z)] + A_{2rpi}\exp[\mathrm{i}(\omega t - k_{2rpix}x - k_{2rpiz}z)]\Big\}\\
\psi_2^S = B_{2ts}\exp[\mathrm{i}(\omega t - k_{2tsx}x + k_{2tsz}z)] + B_{2rs}\exp[\mathrm{i}(\omega t - k_{2rsx}x - k_{2rsz}z)]
\end{cases}\\
&\mathrm{II}:\begin{cases}
\varphi_6^S = \sum\limits_{i=1}^{3}\Big\{A_{6tpi}\exp[\mathrm{i}(\omega t - k_{6tpix}x + k_{6tpiz}z)] + A_{6rpi}\exp[\mathrm{i}(\omega t - k_{6rpix}x - k_{6rpiz}z)]\Big\}\\
\psi_6^S = B_{6ts}\exp[\mathrm{i}(\omega t - k_{6tsx}x + k_{6tsz}z)] + B_{6rs}\exp[\mathrm{i}(\omega t - k_{6rsx}x - k_{6rsz}z)]
\end{cases}
\end{aligned} \tag{4.2}$$

The liquid and gas phases can be indicated as

$$\begin{aligned}
&\mathrm{I}:\begin{cases}
\varphi_2^F = \sum\limits_{i=1}^{3}\delta_{Fi}^{\mathrm{I}}\Big\{A_{2tpi}\exp[\mathrm{i}(\omega t - k_{2tpix}x + k_{2tpiz}z)] + A_{2rpi}\exp[\mathrm{i}(\omega t - k_{2rpix}x - k_{2rpiz}z)]\Big\}\\
\psi_2^F = \delta_{FS}^{\mathrm{I}}\Big\{B_{2ts}\exp[\mathrm{i}(\omega t - k_{2tsx}x + k_{2tsz}z)] + B_{2rs}\exp[\mathrm{i}(\omega t - k_{2rsx}x - k_{2rsz}z)]\Big\}
\end{cases}\\
&\mathrm{II}:\begin{cases}
\varphi_6^F = \sum\limits_{i=1}^{3}\delta_{Fi}^{\mathrm{II}}\Big\{A_{6tpi}\exp[\mathrm{i}(\omega t - k_{6tpix}x + k_{6tpiz}z)] + A_{6rpi}\exp[\mathrm{i}(\omega t - k_{6rpix}x - k_{6rpiz}z)]\Big\}\\
\psi_6^F = \delta_{FS}^{\mathrm{II}}\Big\{B_{6ts}\exp[\mathrm{i}(\omega t - k_{6tsx}x + k_{6tsz}z)] + B_{6rs}\exp[\mathrm{i}(\omega t - k_{6rsx}x - k_{6rsz}z)]\Big\}
\end{cases}
\end{aligned} \tag{4.3}$$

(3) In the WIB_1, WIB_2 and WIB_3

$$\begin{aligned}
&\mathrm{WIB}_1:\begin{cases}
\varphi_3^{w1} = A_{3tp}\exp[\mathrm{i}(\omega t - k_{3tpx}x + k_{3tpz}z)] + A_{3rp}\exp[\mathrm{i}(\omega t - k_{3rpx}x - k_{3rpz}z)]\\
\psi_3^{w1} = B_{3ts}\exp[\mathrm{i}(\omega t - k_{3tsx}x + k_{3tsz}z)] + B_{3rs}\exp[\mathrm{i}(\omega t - k_{3rsx}x - k_{3rsz}z)]
\end{cases}\\
&\mathrm{WIB}_2:\begin{cases}
\varphi_4^{w2} = A_{4tp}\exp[\mathrm{i}(\omega t - k_{4tpx}x + k_{4tpz}z)] + A_{4rp}\exp[\mathrm{i}(\omega t - k_{4rpx}x - k_{4rpz}z)]\\
\psi_4^{w2} = B_{4ts}\exp[\mathrm{i}(\omega t - k_{4tsx}x + k_{4tsz}z)] + B_{4rs}\exp[\mathrm{i}(\omega t - k_{4rsx}x - k_{4rsz}z)]
\end{cases}\\
&\mathrm{WIB}_3:\begin{cases}
\varphi_5^{w3} = A_{5tp}\exp[\mathrm{i}(\omega t - k_{5tpx}x + k_{5tpz}z)] + A_{5rp}\exp[\mathrm{i}(\omega t - k_{5rpx}x - k_{5rpz}z)]\\
\psi_5^{w3} = B_{5ts}\exp[\mathrm{i}(\omega t - k_{5tsx}x + k_{5tsz}z)] + B_{5rs}\exp[\mathrm{i}(\omega t - k_{5rsx}x - k_{5rsz}z)]
\end{cases}
\end{aligned} \tag{4.4}$$

where the superscript e indicates the bedrock, $\delta_{Fi}^{\mathrm{I,II}}$ $(i = 1, 2, 3)$ are the three compression wave participation parameters of the F phase. $\delta_{FS}^{\mathrm{I,II}}$ is the shear wave participation parameters of the

F phase. The subscripts i, t and r refer to quantities corresponding to the incidence, transmission and reflection, respectively. k_{1ipx}, k_{1rpx}, k_{2tpix}, k_{2rpix}, k_{2tsx}, k_{2rsx}, k_{3tpx}, k_{3rpx}, k_{3tsx}, k_{3rsx}, k_{4tpx}, k_{4rpx}, k_{4tsx}, k_{4rsx}, k_{5tpx}, k_{5rpx}, k_{5tsx}, k_{5rsx}, k_{6tpix}, k_{6rpix}, k_{6tsx}, k_{6rsx} are the waves mentioned above that must have equal wave numbers in the x-direction, respectively. The Snell law describing the relations between the angles of incidence, reflection and transmission are given by

$$\begin{aligned} k_{1isx} &= k_{1rpx} = k_{1rsz} = k_{2tpix} = k_{2rpix} = k_{2tsx} = k_{2rsx} = k_{6tpix} = k_{6rpix} \\ &= k_{6tsx} = k_{6rsx} = k_x = k_s \sin\varphi \end{aligned} \tag{4.5}$$

4.2. Boundary conditions

The amplitudes A_{1rp}, B_{1rs}, A_{2tpi}, A_{2rpi}, B_{2ts}, B_{2rs}, A_{3tp}, A_{3rp}, B_{3ts}, B_{3rs}, A_{4tp}, A_{4rp}, B_{4ts}, B_{4rs}, A_{5tp}, A_{5rp}, B_{5ts}, B_{5rs}, A_{6tpi}, A_{6rpi}, B_{6ts}, B_{6rs} can be determined by boundary conditions at the interfaces. The boundary conditions of interfaces are: continuities of normal stresses, tangential stress, normal displacements and tangential displacement.

— At the interface between the bedrock and unsaturated soil layer I

$$\begin{aligned} &\sigma^e_{zz}\Big|_{z=H} = \sigma^S_{zz\mathrm{I}}\Big|_{z=H} + \sigma^L_{zz\mathrm{I}}\Big|_{z=H} + \sigma^G_{zz\mathrm{I}}\Big|_{z=H} \qquad && \sigma^e_{xz}\Big|_{z=H} = \sigma^S_{xz\mathrm{I}}\Big|_{z=H} \\ &u^e_z\Big|_{z=H} = u^S_{z\mathrm{I}}\Big|_{z=H} = u^L_{z\mathrm{I}}\Big|_{z=H} = u^G_{z\mathrm{I}}\Big|_{z=H} && u^e_x\Big|_{z=H} = u^S_{x\mathrm{I}}\Big|_{z=H} \end{aligned} \tag{4.6}$$

— At the interface between WIB_1 and unsaturated soil layer I

$$\begin{aligned} &\sigma^{w1}_{zz}\Big|_{z=H-H_1} = \sigma^S_{zz\mathrm{I}}\Big|_{z=H-H_1} + \sigma^L_{zz\mathrm{I}}\Big|_{z=H-H_1} + \sigma^G_{zz\mathrm{I}}\Big|_{z=H-H_1} \qquad && \sigma^{w1}_{xz}\Big|_{z=H-H_1} = \sigma^S_{xz\mathrm{I}}\Big|_{z=H-H_1} \\ &u^{w1}_z\Big|_{z=H-H_1} = u^S_{z\mathrm{I}}\Big|_{z=H-H_1} = u^L_{z\mathrm{I}}\Big|_{z=H-H_1} = u^G_{z\mathrm{I}}\Big|_{z=H-H_1} && u^{w1}_x\Big|_{z=H-H_1} = u^S_{x\mathrm{I}}\Big|_{z=H-H_1} \end{aligned} \tag{4.7}$$

— At the interface between WIB_1 and WIB_2

$$\begin{aligned} &\sigma^{w2}_{zz}\Big|_{z=H_2+H_{w2}+H_{w3}} = \sigma^{w1}_{zz}\Big|_{z=H_2+H_{w2}+H_{w3}} \qquad && \sigma^{w2}_{xz}\Big|_{z=H_2+H_{w2}+H_{w3}} = \sigma^{w1}_{xz}\Big|_{z=H_2+H_{w2}+H_{w3}} \\ &u^{w2}_z\Big|_{z=H_2+H_{w2}+H_{w3}} = u^{w1}_z\Big|_{z=H_2+H_{w2}+H_{w3}} && u^{w2}_x\Big|_{z=H_2+H_{w2}+H_{w3}} = u^{w1}_x\Big|_{z=H_2+H_{w2}+H_{w3}} \end{aligned} \tag{4.8}$$

— At the interface between WIB_2 and WIB_3

$$\begin{aligned} &\sigma^{w3}_{zz}\Big|_{z=H_2+H_{w3}} = \sigma^{w2}_{zz}\Big|_{z=H_+H_{w3}} \qquad && \sigma^{w3}_{xz}\Big|_{z=H_2+H_{w2}+H_{w3}} = \sigma^{w2}_{xz}\Big|_{z=H_2+H_{w3}} \\ &u^{w3}_z\Big|_{z=H_2+H_{w3}} = u^{w2}_z\Big|_{z=H_2+H_{w3}} && u^{w3}_x\Big|_{z=H_2+H_{w3}} = u^{w2}_x\Big|_{z=H_2+H_{w3}} \end{aligned} \tag{4.9}$$

— At the interface between WIB_3 and unsaturated soil layer II

$$\begin{aligned} &\sigma^{w3}_{zz}\Big|_{z=H_2} = \sigma^S_{zz\mathrm{II}}\Big|_{z=H_2} + \sigma^L_{zz\mathrm{II}}\Big|_{z=H_2} + \sigma^G_{zz\mathrm{II}}\Big|_{z=H_2} \qquad && \sigma^{w3}_{xz}\Big|_{z=H_2} = \sigma^S_{xz\mathrm{II}}\Big|_{z=H_2} \\ &u^{w3}_z\Big|_{z=H_2} = u^S_{z\mathrm{II}}\Big|_{z=H_2} = u^L_{z\mathrm{II}}\Big|_{z=H_2} = u^G_{z\mathrm{II}}\Big|_{z=H_2} && u^{w3}_x\Big|_{z=H_2} = u^S_{x\mathrm{II}}\Big|_{z=H_2} \end{aligned} \tag{4.10}$$

— At the free surface ($z = 0$)

$$\sigma^S_{zz\mathrm{II}}\Big|_{z=0} = \sigma^L_{zz\mathrm{II}}\Big|_{z=0} = \sigma^G_{zz\mathrm{II}}\Big|_{z=0} = \sigma^S_{xz\mathrm{II}}\Big|_{z=0} = 0 \tag{4.11}$$

With the introduction of a potential function, where the expressions of the potential function are detailed in the literature (Jiang and Ma, 2022), the linear systems can be obtained by substituting Eqs. (4.1)-(4.4) into Eqs. (4.6)-(4.11) and Snell law (4.5) as follows

$$\mathbf{MN} = B_{1is}\mathbf{Q} \tag{4.12}$$

where $\mathbf{M}$ is the coefficient matrix of wave amplitudes in $\mathbf{N}$, $\mathbf{Q}$ is the coefficient matrix of wave amplitude of the incident S-wave, and

$$\begin{aligned}\mathbf{N} = [&A_{1rp}, B_{1rs}, A_{2tpi}, B_{2ts}, A_{2rpi}, B_{2rs}, A_{3tp}, B_{3ts}, A_{3rp}, B_{3rs}, A_{4tp}, B_{4ts}, A_{4rp}, B_{4rs},\\ &A_{5tp}, B_{5ts}, A_{5rp}, B_{5rs}, A_{6tpi}, B_{6ts}, A_{6rpi}, B_{6rs}]^{\mathrm{T}}\end{aligned}$$

Supposing $B_{1is} = 1$, the values of the elements in the matrix $\mathbf{N}$ can be derived, thereby the displacements and stresses at each point in the wavefield can be calculated. This work mainly considers the vertical displacement at the surface, which can be obtained by substituting Eqs. (4.2) into the potential function

$$u_z = \left|\sum_{j=1}^{3}(k_{6tpjz}A_{6tpj} - k_{6rpjz}A_{6rpj}) - k_{6tsx}B_{6ts} - k_{6rsx}B_{6rs}\right| \tag{4.13}$$

5. Numerical analysis

5.1. Model verification

The ground motion of the unsaturated soil layer-bedrock system excited by the S-wave, as investigated by Li *et al.* (2018), is chosen to verify the accuracy of this work. Taking the parameters consistent with the literature (Li *et al.*, 2018), variation curves of the surface vertical displacement amplification coefficient with the S-wave angle of incidence for $n = 0.3$, $Sr = 0.8$ and $\omega/\omega_1 = 1.0$ are plotted in Fig. 2. It is shown in Fig. 2 that the present solution is in good consistency with the literature solution, which verifies the validity of the present method.

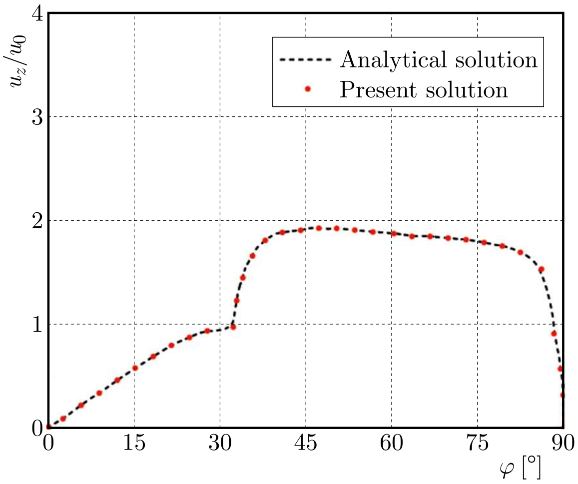

Fig. 2. Comparison between the solution of this paper and the solution from literature

5.2. Effect of the wave impedance ratio on the isolation capacity of a composite multilayer WIB

In this Section, MATLAB is used to analyze the effect of interlayers wave impedance ratio between WIB_1 and unsaturated soil, WIB_1 and WIB_2, and WIB_2 and WIB_3 on the surface displacement. The physical parameters were selected from the literature (Chen *et al.*, 2011), the parameters of the unsaturated foundation are shown in Table 1 and the parameters of the bedrock and composite multilayer WIB are shown in Table 2.

Table 1. Physical and mechanical parameters of the unsaturated porous medium

Material parameters	Porosity	Density of			Bulk modulus of		
		soil particle	liquid	gas	soil particle	liquid	gas
Symbol [unit]	n [–]	ρ_S [kg/m^3]	ρ_L [kg/m^3]	ρ_G [kg/m^3]	K_S [GPa]	K_L [GPa]	K_G [MPa]
Magnitude	0.3	2700	1000	1.2	35	2.2	0.1

Material parameters	Intrinsic permeabil. of the soil	Viscosity coefficient of liquid	Viscosity coefficient of gas	Lamé constant	Lamé constant	Van Genuchten parameter	Van Genuchten parameter
Symbol [unit]	k [m^2]	η^L [Pa·s]	η^G [Pa·s]	λ_S [GPa]	μ_S [GPa]	m_{vg} [–]	α_{vg} [Pa^{-1}]
Magnitude	$3.0 \cdot 10^{-13}$	0.001	$1.8 \cdot 10^{-5}$	9.0	4.0	0.5	0.0001

Table 2. Physical and mechanical parameters of the WIB and bedrock

Material parameters	Lamé constants in GPa							
Symbol	μ_{w1}	λ_{w1}	μ_{w2}	λ_{w2}	μ_{w3}	λ_{w3}	μ_e	λ_e
Magnitude	8.0	12.0	8.0	12.0	8.0	12.0	8.0	12.0

When the S-wave incides from the single-phase bedrock medium to the unsaturated porous medium, there exists a critical angle of incidence φ_{cr}, and the wave velocities of P- and S-waves can be obtained from the formula in elastic mechanics: $v_{is} = \sqrt{\mu_e/\rho_e} = 1721\,\mathrm{m/s}$, $v_{rp} = \sqrt{(\lambda_e + 2\mu_e)/\rho_e} = 3220\,\mathrm{m/s}$. In which $\varphi_{cr} = \sin^{-1}(v_{is}/v_{rp}) \approx 32.3°$. The transmission and reflection of the wave will disappear when the incident angle of the S-wave exceeds the critical angle, so the variation range of the incident angle is taken as 0°-30° in the later discussion.

According to the literature (Sun and Li, 2011), it is known that the definition of wave impedance is the multiplication of velocity v and density ρ. The ratio between the first medium wave impedance $\rho_1 v_1$ and the second medium wave impedance $\rho_2 v_2$ is the wave impedance ratio, which can be expressed as: $\gamma = \rho_1 v_1/\rho_2 v_2$. The wave impedance of the unsaturated soil is Z_0, the wave impedance of WIB_1 is Z_1, the wave impedance of WIB_2 is Z_2 and the wave impedance of WIB_3 is Z_3. Then the wave impedance ratio at the interface between the WIB_1 and unsaturated soil layer would be

$$\gamma_1 = \frac{Z_1}{Z_0} = \frac{\sqrt{(\lambda_{w1} + 2\mu_{w1})\rho_{w1}}}{\rho_s v_{p1}}$$

the wave impedance ratio at the interface between WIB_2 and WIB_1 would be

$$\gamma_2 = \frac{Z_2}{Z_1} = \sqrt{\frac{(\lambda_{w2} + 2\mu_{w2})\rho_{w2}}{(\lambda_{w1} + 2\mu_{w1})\rho_{w1}}}$$

the wave impedance ratio at the interface between WIB_3 and WIB_2 would be

$$\gamma_3 = \frac{Z_3}{Z_2} = \sqrt{\frac{(\lambda_{w3} + 2\mu_{w3})\rho_{w3}}{(\lambda_{w2} + 2\mu_{w2})\rho_{w2}}}$$

According to the formula of wave impedance ratio, the material parameters which affect the wave impedance ratio are mainly the density and Lamé constant. The surface vertical displacement under simultaneous variation of the wave impedance ratio between material layers in the range of 0.5-20 is calculated by MATLAB. The wave impedance ratio corresponding to the minimum surface vertical displacement will be selected to determine the material parameters for vibration isolation design: density and shear modulus of the composite multilayer WIB. Six cases of density of WIB are discussed as follows:

Case 1: $\rho_{w1} < \rho_{w2} < \rho_{w3}$ which $\rho_{w1} = 2000\,\mathrm{kg/m^3}$, $\rho_{w2} = 2400\,\mathrm{kg/m^3}$, $\rho_{w3} = 2700\,\mathrm{kg/m^3}$
Case 2: $\rho_{w1} < \rho_{w2} > \rho_{w3}$ which $\rho_{w1} = 2000\,\mathrm{kg/m^3}$, $\rho_{w2} = 2700\,\mathrm{kg/m^3}$, $\rho_{w3} = 2400\,\mathrm{kg/m^3}$
Case 3: $\rho_{w1} > \rho_{w2} < \rho_{w3}$ which $\rho_{w1} = 2400\,\mathrm{kg/m^3}$, $\rho_{w2} = 2000\,\mathrm{kg/m^3}$, $\rho_{w3} = 2700\,\mathrm{kg/m^3}$
Case 4: $\rho_{w1} < \rho_{w2} > \rho_{w3}$ which $\rho_{w1} = 2400\,\mathrm{kg/m^3}$, $\rho_{w2} = 2700\,\mathrm{kg/m^3}$, $\rho_{w3} = 2000\,\mathrm{kg/m^3}$
Case 5: $\rho_{w1} > \rho_{w2} > \rho_{w3}$ which $\rho_{w1} = 2700\,\mathrm{kg/m^3}$, $\rho_{w2} = 2400\,\mathrm{kg/m^3}$, $\rho_{w3} = 2000\,\mathrm{kg/m^3}$
Case 6: $\rho_{w1} > \rho_{w2} < \rho_{w3}$ which $\rho_{w1} = 2700\,\mathrm{kg/m^3}$, $\rho_{w2} = 2000\,\mathrm{kg/m^3}$, $\rho_{w3} = 2400\,\mathrm{kg/m^3}$

Considering the saturation $Sr = 0.8$, incidence frequency $\omega = 10\,\mathrm{Hz}$, angle of incidence $\varphi = 30°$, thickness of the composite multilayer WIB $H_{w1} = H_{w2} = H_{w3} = 0.3\,\mathrm{m}$, and burial depth $H_2 = 1.0\,\mathrm{m}$, 3D curves of the surface vertical displacement with simultaneous variation of the wave impedance ratio γ_1, γ_2 and γ_3 under six cases are plotted in Fig. 3, respectively. As shown in Fig. 3, the surface vertical displacement decreases with an increase in the wave impedance ratio, and the amplitude of the surface vertical displacement reaches the minimum when the wave impedance ratio increases to a certain degree. In addition, it can also be seen from the values of the axes in the right side of Fig. 3 that the range of the vertical displacement amplitude at the surface in Case 3 is the minimum. The minimum value of the surface vertical displacement and the corresponding wave impedance for six cases are calculated as follows:

(1) when $\rho_{w1} < \rho_{w2} < \rho_{w3}$, $\gamma_1 = 2.0$, $\gamma_2 = 11.5$, $\gamma_3 = 19.5$, $u_{z\,min} = 9.35 \cdot 10^{-12}$,m
(2) when $\rho_{w1} < \rho_{w2} > \rho_{w3}$, $\gamma_1 = 16.0$, $\gamma_2 = 2.5$, $\gamma_3 = 10.5$, $u_{z\,min} = 5.14 \cdot 10^{-10}\,\mathrm{m}$
(3) when $\rho_{w1} > \rho_{w2} < \rho_{w3}$, $\gamma_1 = 16.0$, $\gamma_2 = 2.5$, $\gamma_3 = 10.5$, $u_{z\,min} = 8.68 \cdot 10^{-12}\,\mathrm{m}$
(4) when $\rho_{w1} < \rho_{w2} > \rho_{w3}$, $\gamma_1 = 14.5$, $\gamma_2 = 11.5$, $\gamma_3 = 13.0$, $u_{z\,min} = 2.33 \cdot 10^{-10}\,\mathrm{m}$
(5) when $\rho_{w1} > \rho_{w2} > \rho_{w3}$, $\gamma_1 = 13.5$, $\gamma_2 = 3.0$, $\gamma_3 = 9.5$, $u_{z\,min} = 8.71 \cdot 10^{-11}\,\mathrm{m}$
(6) when $\rho_{w1} > \rho_{w2} < \rho_{w3}$, $\gamma_1 = 6.5$, $\gamma_2 = 16.5$, $\gamma_3 = 4.0$, $u_{z\,min} = 4.39 \cdot 10^{-8}\,\mathrm{m}$

The above six density cases show that the surface vertical displacement obtained in Case 3 is the minimum value. At this time, the composite multilayer WIB achieves the most effective isolation effect. And the shear modulus of the composite multilayer WIB, in this case, can be back-calculated from the wave impedance ratio: $\mu_{w1} = 3.53 \cdot 10^{11}\,\mathrm{Pa}$ for WIB_1, $\mu_{w2} = 1.17 \cdot 10^{14}\,\mathrm{Pa}$ for WIB_2, and $\mu_{w3} = 1.39 \cdot 10^{15}\,\mathrm{Pa}$ for WIB_3. In summary, the calculation can find the wave impedance ratio corresponding to the optimal vibration isolation effect of the composite multilayer WIB to determine the material parameters of the composite multilayer WIB and derive design guidelines for multilayer vibration barriers. In the design of a multilayer vibration barrier, physical material parameters with greater density on both sides, smaller density in the center and the shear modulus increasing gradually from the bottom to the top can be selected to achieve the optimal vibration isolation effect.

5.3. Analysis of vibration isolation law for the composite multilayer WIB

In this Section, the material parameters are taken from Case 3, which is discussed in Section 5.2 when the optimal isolation effect of the composite multilayer WIB is achieved, and the vibration isolation performance is analyzed. For the evaluation of the vibration isolation effect of the composite multilayer WIB, this paper adopts the amplitude attenuation ratio A_R proposed by Woods *et al.* (1974) to evaluate its vibration isolation effect. The formula is expressed as: $A_R = u_z/u_z^*$, where u_z is the surface vertical displacement after installing the WIB in the

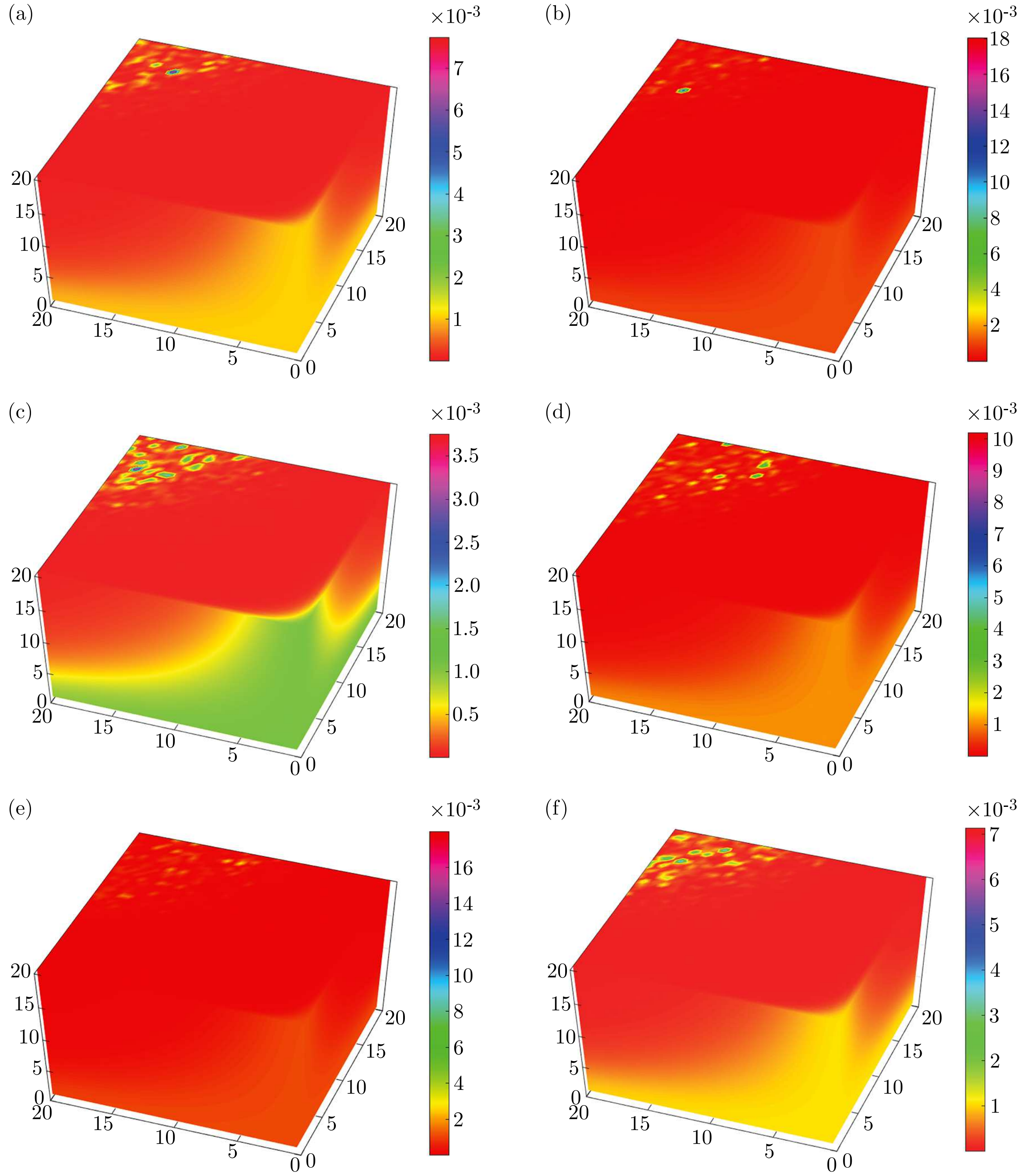

Fig. 3. 3D curves of the vertical surface displacement with simultaneous variation of the wave impedance ratio: (a) Case 1, (b) Case 2, (c) Case 3, (d) Case 4, (e) Case 5, (f) Case 6

unsaturated foundation, u_z^* is the surface vertical displacement without installation of WIB in the unsaturated foundation.

Figure 4 plots the comparison of the isolation effect of a single-layer WIB and the composite multilayer WIB for burial depth $H_2 = 1.0\,\mathrm{m}$, saturation $Sr = 0.8$, incidence frequency $\omega = 10\,\mathrm{Hz}$, total thickness of the soil layer $H = 20\,\mathrm{m}$ and other parameters taken from Table 1. The material parameters of the composite multilayer WIB are taken from Case 3. The material parameters of the single-layer WIB are taken as corresponding to those of each layer in the composite multilayer WIB. Accordingly, thickness of the single-layer WIB is 0.9 m, and density and shear modulus are as follows: (1) $\rho_w = 2000\,\mathrm{kg/m^3}$, $\mu_w = 1.17 \cdot 10^{14}\,\mathrm{Pa}$; (2) $\rho_w = 2400\,\mathrm{kg/m^3}$, $\mu_w = 3.53 \cdot 10^{11}\,\mathrm{Pa}$;

(3) $\rho_w = 2700\,\mathrm{kg/m^3}$, $\mu_w = 1.39 \cdot 10^{15}$ Pa. It can be seen from Fig. 4 that the isolation effect of the single-layer homogeneous WIB with three kinds of materials is not as good as the composite multilayer WIB. For the calculation in this paper, the effective isolation angle range of the single-layer WIB is 12°-28° when $\rho_w = 2000\,\mathrm{kg/m^3}$, and the average amplitude attenuation ratio is $A_R = 0.678$ in this range. When $\rho_w = 2400\,\mathrm{kg/m^3}$, the effective isolation angle range of the single-layer WIB is 10°-29°, and the average amplitude attenuation ratio in this range $A_R = 0.509$. When $\rho_w = 2700\,\mathrm{kg/m^3}$, the effective isolation angle range of the single-layer WIB is 4°-28°, and the average amplitude attenuation coefficient in this range is $A_R = 0.36$. The composite multilayer WIB has effective vibration isolation in the critical angle range and its average amplitude attenuation ratio is $A_R = 0.093$. In summary, the vibration isolation efficiency of the composite multilayer WIB is enhanced by 86.28% over the single-layer WIB for $\rho_w = 2000\,\mathrm{kg/m^3}$, 81.73% over the single-layer WIB for $\rho_w = 2400\,\mathrm{kg/m^3}$, and 74.17% over the single-layer WIB for $\rho_w = 2700\,\mathrm{kg/m^3}$. Therefore, with the same thickness of vibration isolation system, the isolation effect of the composite multilayer WIB is significantly better than that of the single-layer homogeneous WIB.

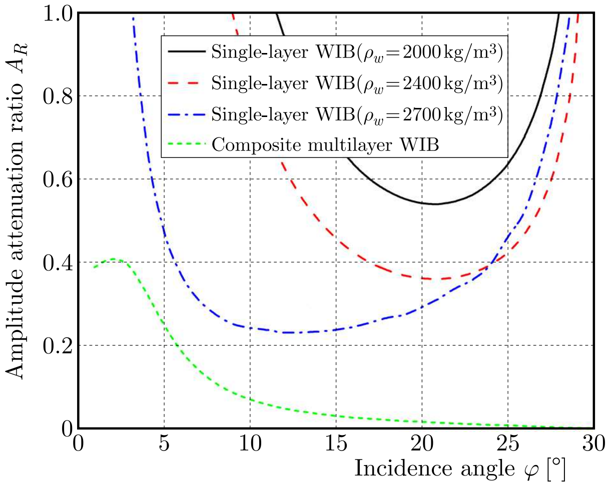

Fig. 4. Comparison of A_R with the angle of incidence for the single-layer and composite multilayer WIB

The effects of the same incidence frequency on the vibration isolation effect of the single-layer and composite multilayer WIB in the unsaturated foundation will be analyzed next. In the analysis, the saturation is 0.8, thickness of the unsaturated soil layer $H = 20$ m, burial depth $H_2 = 1.0$ m, thickness of single-layer and composite multilayer WIB 0.9 m, and other parameters are taken from Table 1. Three cases of the incidence frequency, $\omega = 10$ Hz, 50 Hz and 100 Hz are considered, respectively. As shown in Fig. 5, the average amplitude attenuation ratio is $A_R = 0.91$ for the single-layer WIB and $A_R = 0.066$ for the composite multilayer WIB when $\omega = 50$ Hz, in which case the isolation efficiency is 92.75% higher than for the single-layer WIB. When $\omega = 100$ Hz, the single-layer WIB vibration isolation fails, its average amplitude attenuation ratio is $A_R = 4.43$ and $A_R = 0.036$ for the composite multilayer WIB, whose isolation efficiency is 99.18% higher than that of the single-layer WIB. Consistently, it is evident that the composite multilayer WIB can improve the defect that the single-layer WIB has only good vibration isolation effect at a low frequency. The composite multilayer WIB can isolate the incidence frequencies at low, medium and high frequencies effectively, and the isolation efficiency gradually increases with an increase in the incidence frequency. Among the common types of environmental vibration in cities, the main vibration frequency caused by tamping is concentrated in 10-20 Hz, the main vibration frequency caused by elevators is within 20-25 Hz, and the main vibration frequency caused by subway is higher, between 50-80 Hz. On the whole, the frequency of environmental vibration will not exceed 100 Hz in general. Thus, the composite multilayer WIB is suitable for isolating common city environmental vibrations, especially those caused by traffic.

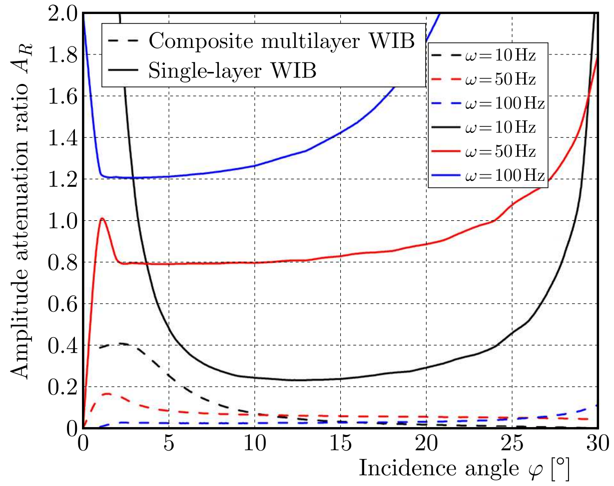

Fig. 5. Variations of the vertical displacement amplitude attenuation ratio at the surface along with ω

The following Section investigates the effect of saturation on the vibration isolation effect of the composite multilayer WIB in the unsaturated foundation for thickness of the soil layer $H = 20\,\mathrm{m}$, burial depth $H_2 = 1.0\,\mathrm{m}$, thickness of the composite multilayer WIB $H_{w1} = H_{w2} = H_{w3} = 0.3\,\mathrm{m}$, incidence frequency $\omega = 10\,\mathrm{Hz}$, and other parameters taken from Table 1. The saturation is $Sr = 0.2$, 0.4, 0.6 and 0.8, respectively. The variation curves of the surface vertical displacement amplitude attenuation ratio with the angle of incidence for different saturations when the composite multilayer WIB is set up in the unsaturated foundation are given in Fig. 6. Firstly, it can be seen from Fig. 6 that the surface vertical displacement amplitude attenuation

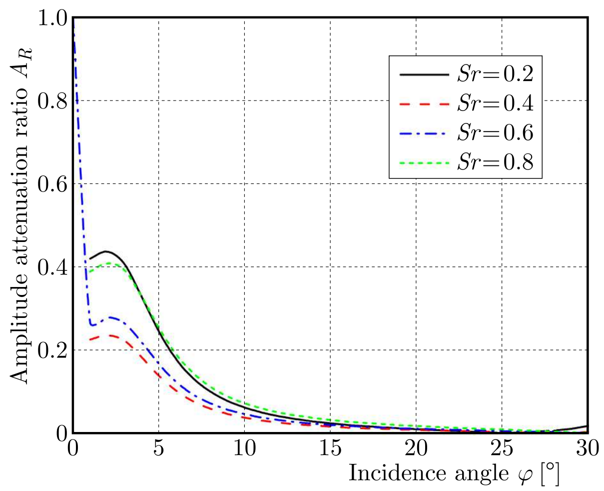

Fig. 6. Variations of the vertical displacement amplitude attenuation ratio at the surface along with Sr

ratio exhibits irregularity with the variation of saturation. When $Sr = 0.2$, the average amplitude attenuation ratio is $A_R = 0.0899$, $A_R = 0.0508$ when $Sr = 0.4$. The vibration isolation effect is 43.49% higher than that for $Sr = 0.2$. The average amplitude attenuation ratio $A_R = 0.0916$ at $Sr = 0.6$ and its vibration isolation effect is 44.54% lower than that for $Sr = 0.4$, whereas the vibration isolation effect at $Sr = 0.8$ is 1.51% lower than that for $Sr = 0.6$. It means that the vibration isolation effect of the composite multilayer WIB in the unsaturated foundation increases and then decreases with an increase of saturation. To sum up, the saturation has a significant effect on the isolation effect of the composite multilayer WIB. It is difficult to simulate the actual situation by simplifying the foundation into a single-phase elastic and two--phase saturated foundation.

6. Conclusion

Combining the wave propagation theory and Snell's theorem, the vibration isolation performance of a composite multilayer WIB in an unsaturated foundation, which is more consistent with reality, is investigated. The vibration isolation performance of the composite multilayer WIB and a single-layer WIB under the same thickness have been compared and analyzed. The influence laws of saturation and incidence frequency on the isolation effect of the composite multilayer WIB in the unsaturated foundation have been investigated. Conclusions can be drawn as follows.

- Physical parameters of large density on both sides and small density in the center and a gradually increasing shear modulus from bottom to top can achieve the optimal isolation effect when designing a composite multilayer vibration barrier.
- Vibration multilayer barriers can isolate common environmental vibration sources in cities, especially, medium and high frequency vibrations caused by traffic. For the same thickness of the vibration isolation system, the isolation effect of the composite multilayer WIB is better than thaf of a single-layer WIB. At a low incidence frequency ($\omega = 10\,\text{Hz}$), the vibration isolation efficiency of the composite multilayer WIB is 86.28% higher than that of the single-layer WIB. At a medium incidence frequency ($\omega = 50\,\text{Hz}$), the vibration isolation efficiency of the composite multilayer WIB is 92.75% higher than that of the single-layer WIB. At a high incidence frequency ($\omega = 100\,\text{Hz}$), the vibration isolation efficiency of the composite multilayer WIB is 99.18% higher than that of the single-layer WIB.
- The isolation effect of the composite multilayer WIB increases and then decreases with an increase of saturation, and gradually increases with an increase of the angle of incidence.

References

1. Borja R.I., 2006, On the mechanical energy and effective stress in saturated and unsaturated porous continua, *International Journal of Solids and Structures*, **43**, 1764-1786

2. Chen W., Xia T., Hu W., 2011, A mixture theory analysis for the surface-wave propagation in an unsaturated porous medium, *International Journal of Solids and Structures*, **48**, 2402-2412

3. Chouw N., Le R., Schmid G., 1991a, An approach to reduce foundation vibrations and soil waves using dynamic transmitting behavior of a soil layer, *Bauingenieur*, **66**, 215-221

4. Chouw N., Le R., Schmid G., 1991b, Propagation of vibration in a soil layer over bedrock, *Engineering Analysis with Boundary Elements*, **8**, 125-131

5. Gao M., Zhang Z.S., Wang C.G., Tian S.P., 2021, Field test on vibration isolation performance by WIB-Duxseal under vertical excitation (in Chinese), *Rock and Soil Mechanics*, **42**, 537-546

6. Jiang Y., Ma Q., 2022, Study on vibration isolation effect of wave impeding block in unsaturated soil under S-wave incidence, *Acta Mechanica*, **233**, 4119-4139

7. Li Z.J., He Z., Tan Y., Xiao J.H., 2011, HWIB isolation analysis of low-frequency vibration from high speed railways by using HWIB (in Chinese), *Journal of Huazhong University of Science and Technology (Natural Science Edition)*, **39**, 34-38

8. Li W., Zheng J., Trifunac M.D., 2018, Saturation effects on ground motion of unsaturated soil layer-bedrock system excited by plane P and SV waves, *Soil Dynamics and Earthquake Engineering*, **110**, 159-172

9. Ma Q., Zhou F., Zhang W., 2019, Vibration isolation of saturated foundations by functionally graded wave impeding block under a moving load, *Journal of the Brazilian Society of Mechanical Sciences and Engineering*, **41**, 1-10

10. Shu J., Ma Q., 2022, Study the propagation characteristics of P_1-wave passing through composite multilayer wave impeding block in unsaturated soil, *The European Physical Journal Plus*, **137**, 1-16

11. Shu J.H, Ma Q., Zhou F.X., Li Q., 2022, Study on the propagation characteristics of P_1 wave passing through wave impeding block in unsaturated soil (in Chinese), *Rock and Mechanics*, **43**, 1135-1146

12. Sun C.Y., Li Z.C., 2011, *The Fundamentals of Seismic Wave Dynamics*, Petroleum Industry Press, Beijing

13. Takemiya H., Jiang J., 1993, Wave impeding effect by buried rigid block and response reduction of dynamically excited pile foundation, *Doboku Gakkai Ronbunshu*, **1993**, 45-52

14. Tian S.P., Gao M., Wang Y., Chen Q.S., 2019, Two dimensional analysis of Duxseal material as active vibration isolation in homogeneous elastic foundation (in Chinese), *Journal of Vibration Engineering*, **32**, 701-711

15. Woods R.D., Barnett N.E., Sagesser R., 1974, Holography – A new tool for soil dynamics, *Journal of the Geotechnical Engineering Division*, **100**, 1231-1247

16. Yang Y.B., Hung H.H., 1997, A parametric study of wave barriers for reduction of train-induced vibrations, *International Journal for Numerical Methods in Engineering*, **40**, 3729-3747

17. Zhou F.X., Ma Q., Lai Y.M., 2016, Ground vibration control with fluid-saturated porous wave impeding blocks (in Chinese), *Journal of Vibration and Shock*, **35**, 96-105

Manuscript received January 9, 2023; accepted for print March 26, 2023